Nano Research
2021, 14(5): 1233–1243

ISSN 1998-0124 CN 11-5974/O4
https://doi.org/10.1007/s12274-020-3140-y

Flagship Review

Self-assembly of semiconductor nanoparticles toward emergent behaviors on fluorescence

Xiao Li[1,2], Zhili Lu[3], and Tie Wang[1,2,4] (✉)

[1] *Beijing National Laboratory for Molecular Sciences, Key Laboratory of Analytical Chemistry for Living Biosystems, Institute of Chemistry, Chinese Academy of Sciences, Beijing 100190, China*
[2] *University of Chinese Academy of Sciences, Beijing 100049, China*
[3] *Key Laboratory of Materials Processing and Mold, Ministry of Education, Zhengzhou University, Zhengzhou 450001, China*
[4] *Life and Health Research Institute, School of Chemistry and Chemical Engineering, Tianjin University of Technology, Tianjin 300384, China*

Received: 13 August 2020 / **Revised:** 21 September 2020 / **Accepted:** 23 September 2020

ABSTRACT

Due to the unique fluorescence characteristics, superstructures from self-assembly of semiconductor nanoparticles have become essential components of material and chemical science, and thus it has broad application potential in displays, single-photon source, sensing, biological tagging and emerging quantum technologies. Superstructure refers to an artificial functional architecture whose length scale is between the quantum scale and the macroscale. When solely treating this complicated stage fitted from less complicated pieces together (basic nanoparticles) and pile speculation on speculation, we must understand the fundamental questions, that is, what the hierarchy or specialization of function is at the stage. The uniqueness of this stage is not the collection of basic nanoparticles, but the behavior that emerges on fluorescence-basically a new type of behavior. Under the angle of view, this study reviews the advances in the fluorescence of individual semiconductor nanoparticles, inter-nanoparticles coupling and thus emergent fluorescence behaviors of assemblies. We also try to present the methodology for seeking emergent behaviors on fluorescence.

KEYWORDS

nanoparticle assembly, optical properties, ordered structures, coupling, emergent

1 Introduction

The colloidal nanoparticles (NPs) of group II–VI, III–V and IV–VI semiconductors have attracted wide attention due to their size-dependent optical and electronic properties in which the exciton, electron and hole are quantum-confined to one or more dimensions [1–3]. Akin to the construction of atomic solid or molecule from atoms, semiconductor NPs could serve as building blocks and be spontaneously packed into superstructures (SPs) by a "bottom-up" approach [4, 5]. The building blocks can be any shape and are generally connected by the weak interaction forces including van der Waals interactions, hydrogen bonds, electrostatic interactions, magnetic interactions, etc [6, 7]. The diversity of SPs parallels with the beauty and richness of atomic solid or molecules and the SPs have become a brand-new category of material with novel fluorescence function for vast applications in displays, single-photon sources, biological tagging, sensing and emerging quantum technologies [8–10]. In atomic solids or molecules, certain properties generate and are considered hierarchical or specialized only when atoms form solids or molecules. For example, ammonia molecules have dipole moments, but no nitrogen and hydrogen atom nucleus have a dipole moment when we look at each atom separately. The connection of nitrogen and the triangle of hydrogens produces a triangular pyramid with the negative and the positive ends. Therefore, it has an electric dipole moment with negative ends, toward the apex of the pyramid. Analogously, the connection of inter-NPs gives rise to the basically new types of behavior that are unique to the NPs and bulk, known as the emergent physical phenomena. The focus of this review is the emergent fluorescence properties of SPs resulting from the assembly of semiconductor NPs.

The emergent properties of the assemblies are consistent with emergent effects in biology. Emergence means that one plus one is not equal to two. In other words, emergence is not the simple collection of properties of single NP. It is a systematic upgrade due to the aggregation of NPs and the inter-NPs connection. Light interaction with the assemblies of NPs is different from that with a single NP. At the scale level of SPs, which is between quantum and macro scale, new concepts, methodologies, and generalizations are necessary, which require the same level of wisdom or inspiration as previous studies on NPs and bulk [11]. The coupling between NPs in SPs is a necessary pathway to trigger the emergent behaviors on fluorescence (Scheme 1).

2 The fluorescence of individual semiconductor NPs

Spontaneous emission is the quantum process that involves a transition from an excited state to a state with lower energy

Address correspondence to wangtie@iccas.ac.cn

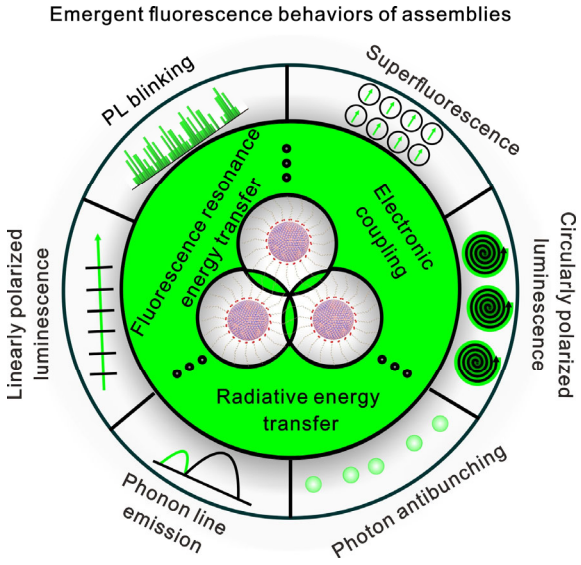

Scheme 1 A schematic diagram of the pathway for assemblies beyond individual building blocks to produce emergent fluorescence properties: coupling.

(typically, the ground state) accompanied by photon emitting. Spontaneous emission facilitates dozens of applications, such as cathode ray tubes, fluorescent tubes, plasma display panels, light-emitting diodes and lasers. Absorption is the quantum process by which photon is absorbed, resulting in an electron to jump from a lower energy level to a higher one. The absorption can be regarded as a reverse process of stimulated emission. It is the fluorescence that is the spontaneous emission of low energy photons excited by high-energy photons. When semiconductor crystals absorb photons that are larger than bandgap, the excited electrons and holes in the valence band are combined through Coulomb interactions to form hot excitons. Under the relaxation mechanism such as phonon vibration, hot excitons lose energy in a short time and become band-edge excitons [12]. In general, edge excitons are generally referred to as excitons in the literature. The excitons in semiconductors also have more precise energy level structures. The excitons distributed in the non-spectral law are called as dark excitons, while the excitons distributed in the spectral law are called as bright excitons or excitons. In semiconductor NPs, such as InAs [13], InP [14], CdSe [15] NPs, the optical transitions of bright singlet exciton usually leads to the photon emission. However, such common sense may not be entirely right. Through to 2018, as for perovskite nanocrystals such as $CsPbBr_3$ [16] and $FAPbBr_3$ NPs [17], triplet state could be optically active and singlet state could be optically passive, due to the strong Rashba effect.

2.1 Size-dependent fluorescence

When the sizes of semiconductor NPs are significantly reduced in the range of the de Broglie wavelength of the electron wave function, the effect of quantum confinement can hardly be ignored for fluorescence. According to the effective mass approximation, there are two essential parameters for quantum confinement: the size of the NPs, D, and the exciton Bohr radius, α_B [18, 19]. For $D \gg \alpha_B$ (the weak confinement regime), the excited electron and hole pair bind together to form an exciton [18]. The energy shift can be calculated by using the reduced mass of the exciton due to low exciton confinement. For $\alpha_B \gg D$ (the strong confinement regime), the electron and hole shall be viewed as separate particles and confinement energies of them should be calculated individually [18]. α_B is the critical size of quantum confinement effect. The exciton Bohr radius is defined as

$$\alpha_B = \frac{\varepsilon}{\varepsilon_v}\frac{m_f \alpha_H}{\mu}$$

where ε_v and ε are the dielectric constants of vacuum and the matter, m_f and μ are the effective masses of the free electron and the exciton respectively, and α_H is the Bohr radius.

The quantum confinement can be one-dimensional, two-dimensional or three-dimensional, which are respectively called quantum wires, quantum plates and quantum dots. As for quantum dots (QD), an analytical approximation for the first excited electronic state [20]

$$E_{QDs} = E_g + \frac{h^2}{8r^2}\left(\frac{1}{m_e} + \frac{1}{m_h}\right) - \frac{1.8e^2}{\varepsilon r}$$

where E_g is bulk bandgap, r is the quantum dot radius, and m_e and m_h are the effective mass of electrons and holes respectively. The Coulomb term $\frac{1.8e^2}{\varepsilon r}$ shifts E_{QDs} to lower energy as r^{-1}, while the quantum localization terms $\frac{h^2}{8r^2}\left(\frac{1}{m_e} + \frac{1}{m_h}\right)$ shift E_{QDs} to higher energy as r^{-2} [20]. Consequently, the apparent bandgap will increase without fail for small enough quantum dots into the regime of quantum confinement. Size control based on the quantum confinement effect benefits luminescence colors size-tunable from ultraviolet (UV) to infrared (IR). On the other hands, this leads to the geometric broadening of linewidth of the emission peak, estimated to be full-width at the maximum, thus reducing the color purity due to the inevitable size polydispersity of NPs even if the synthesis conditions (such as the purity and concentration of raw materials, suitable synthetic routes, reaction temperature, et al.) are strictly controlled. To date, as for toxic CdSe NPs, the narrowest linewidth is in the order of 20 nm, while it is challenging to achieve a value less than 36 nm for nontoxic InP-based NPs by alloying [21, 22]. The other add-on of size-tunable luminescence colors is the inhomogeneity of fluorescence quantum yield among the different sizes because of the changes in the confinement energy and differences in the effective mass of electrons and holes from the strong to the weak confinement regime.

2.2 Surface dependent fluorescence

All NPs feature the high surface-area-to-volume ratio, which means their surfaces play the dominant roles in fluorescence processes [23, 24]. The localized midgap states, induced by the undercoordinated or naked surface atoms with dangling bonds, behave as traps for exciton, electrons, or holes relaxation from the band edge, which quenches intrinsic emission. Excess ion sites on the surface also introduce the extra short or long lifetime channels for the excitons, which reduces the quantum yield of radiative excitons [25–27]. Upon review, identified ligands can eliminate of mid-gap trap states to induce unity single-channel radiative decay of excitons such as primary amines for the CdSe NPs [25]. Surface passivation by ligands usually appears on the specific crystal facets. Tertiary phosphines associating with Se terminated (0001) surface of CdSe NPs exert a dramatic enhancement in photoluminescence (PL) quantum yield [28, 29]. The existence of surface OH^- groups of oleic acid stabilizes the PbS (111) facets [30]. The fluorescence intensity of ligand-passivated NPs is not entirely linear with the coverage of surface ligand. Meanwhile, new mid-gap electronic states could be introduced by some ligands, which, for example, increases the rate of non-radiative decay-alkanethiol ligands quenching

luminescence of CdSe NPs by fast hole trapping [31].

When binding functional molecular, there exists a two-way transfer of energy across semiconductor NPs–molecular interfaces. The orbital motion and spin of the carriers are usually strongly coupled in semiconductors with fine structure. The mixed-spin character of NPs implies that the ligands could extract triplet exciton energy directly from the initially excited state or donate its excitons.

Binding molecules as the triplet excited-state donor could serve as the sensitizer. In 2014, dexter triplets exciton was reported to transfer from the surface organic semiconductor molecular to inorganic semiconductor [32, 33]. Dexter energy transfer is a short-range energy transfer in which the energy of excited states of acceptor materials is equal to or less than that of donor materials. Thompson et al. [32] showed that colloidal PbS nanocrystals harvested the triplet excitons of the attached molecule located at the near-infrared and produced singlet fission in binding molecular tetracene, with a transfer efficiency of at least (90 ± 13)%.

The reverse triplet-energy-transfer process by Dexter-type triplet–triplet energy transfer or triplet-triplet annihilation (TTA) was confirmed in 2016 [34, 35]. With NPs as the triplet sensitizer, surface molecular could serve as an acceptor. Mongin et al. [34] reported interfacial Dexter triplet–triplet energy transfer from CdSe nanocrystals as light-absorbing source excited by green light into surface-anchored polyaromatic carboxylic acid triplet acceptors. The surface organic acceptors of the NPs harvested efficiently from triplet excitons of CdSe NPs with near quantitative yield. On the other hand, TTA processes can cooccur with PbS NPs sensitizer under an appropriate fine structure for infrared-to-visible upconversion [35]. When excited at a wavelength of 808 nm, two excited excitons of the NPs are converted to one higher-energy state in the emitter of dibenzotetraphenylperiflanthene through the annihilator rubrene since the first excited triplet state is positioned for infrared sensitization. Sensitizer-annihilator-emitter of nanocrystals was built for upward channel pushing the electron into the high energy of singlet states by exchanging the electrons between two triplet molecules.

Triplet excitons in surface-bound acceptor molecules collected from CdSe nanocrystals could endothermically reverse into CdSe nanocrystals by designing the CdSe nanocrystal–acceptor energy gap. For example, Mongin et al. [36] reported that CdSe nanocrystals in conjunction with 1-pyrene carboxylic acid molecular underwent thermally activated delayed photoluminescence. This thermally repopulated photoluminescent state between NPs and molecules is akin to the bidirectional reverse intersystem crossing between singlets and triplets in thermally activated delayed photoluminescence molecules. Formation of triplet excited state of the resulting 1-pyrene carboxylic acid was confirmed by monitoring the sensitized $T_1 \rightarrow T_n$ transition centered at 430 nm employing transient absorption. When the energy gap between the NPs excited state and the 1-pyrene carboxylic acid triplet state is small, the triplet state of 1-pyrene carboxylic acid as a reservoir could reverse transfer to the triplet state of nanocrystals again. The observation of delayed CdSe emission verified the reverse TTET process.

3 The pathway for assemblies beyond individual building blocks to produce emergent fluorescence properties: Coupling

Semiconductor NPs assemblies hold promise for the study and eventual control of specific fluorescence-related phenomena that are hard to realize in classic solids and individual nanocrystals. The formation of spot patterns often accompanies the emergence of complex organisms. The assembly of nanocrystals brings about the stacking of geometric particles in physical space, which provides a natural advantage for the emergence of the assemblies. They exhibit emergent properties altered from those of the component NPs due to coupling molding the emitting of light. The coupling between NPs strongly influences the energy distribution among NPs in artificial solids. To achieve emergent fluorescence properties of assemblies beyond that of individual building blocks, coupling stepped into our eyes. The coupling of building blocks in SPs includes principally radiative energy transfer, fluorescence resonance energy transfer (FRET) and electronic coupling processes (Fig. 1). All of them result from the function of the inter-NPs separation distance and media. The shape effect of building blocks mainly causes variation of the contact area and coupling strength in different directions. Compared with quantum dots and nanowires, nanoplatelets have a larger coupling area in two dimensions [37].

3.1 Radiative energy transfer

Radiative energy transfer is an optical phenomenon of energy transfer based on electromagnetic radiation by light–matter interaction. Photons emitted by a single building block could be absorbed, reemitted and scattered many times by the medium-surrounding building blocks. Highly refractive nanoparticles with distinctive shape (such as nanocones, nanorings, nanobowls, et al.) can serve as nanoantennas and direct the light propagation to the targeted layers or device [38]. In hybrid waveguide structure, large Stokes-shift of NPs usually suppresses the reabsorption to lower the "randomization" of the light propagation direction up to tens of centimeters [39, 40].

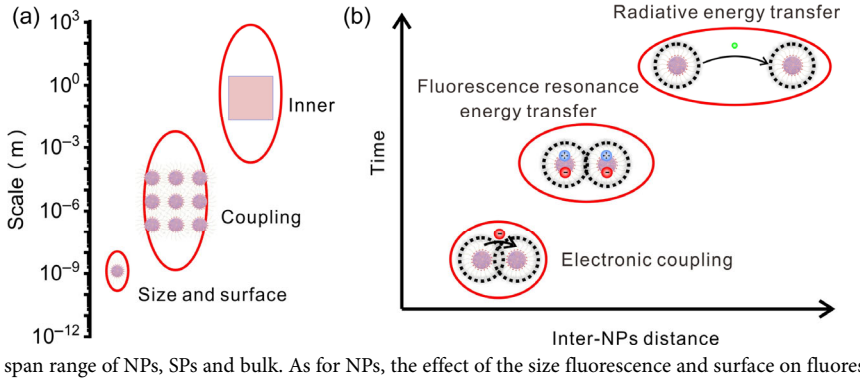

Figure 1 (a) General scale span range of NPs, SPs and bulk. As for NPs, the effect of the size fluorescence and surface on fluorescence can not be ignored. As for bulk, interior space occupies more influence weight than the surface for fluorescence. Compared with the others, the biggest difference of SPs is the connection-related coupling between nanoparticles. (b) Coupling is the function of the inter-NPs separation distance. Radiative energy transfer could span the long distance. However, fluorescence resonance energy transfer and electronic coupling are the relatively short-range process of nearby NPs.

3.2 Fluorescence resonance energy transfer

In classical physics, FRET is the mechanism for electronic "communication" between the donor and acceptor of NPs (D–A pairs) through long-range incoherent dipole–dipole interactions (Fig. 2) [41]. When the D–A pairs have isotropic dipole states, FRET rate is a function of the D–A spectral overlap, which has the r^{-6} dependence on the separation r of D–A.

$$k_T(r) = \frac{1}{\tau_D}\left(\frac{R}{r}\right)^6$$

where τ_D is the decay time of the donor in the absence of acceptor, r is the D–A distance, and R is the Förster distance. Förster distances range from 20 to 90 Å. For example, CdSe NPs were found that the electronic coupling energy drops to nearly zero at inter-NPs distances of about 7 nm [42]. When the absorption spectrum of acceptor overlaps with the emission spectrum of the donor appropriately and the D–A distance is comparable to R, FRET must be considered in the assemblies. The FRET process does not involve reabsorption of photons of neighboring NPs, but rather D–A dipoles resonance with a similar frequency. When the free orientation of D–A dipole in three dimensions changes to the confined direction along one or two dimensions, the strength of FRET can be modified. For example, when CdSe nanoplatelets as acceptor change from the face-down into edge-up orientation pairing with spherical CdZnS/ZnS NPs as donors, the resulting energy transfer from the NPs could be significantly accelerated due to the enhancement of the dipole–dipole interaction factor [43]. The relative geometrical orientation of D–A dipoles serves as another parameter to tune FRET. FRET could work between chemically identical NPs called homo-FRET, which typically occurs in NPs with small Stokes shifts. Multichannel energy transfer based on multiple donors can further improve incident light utilization efficiency and FRET efficiency [44, 45].

3.3 Electronic coupling

On the contrary to the long-range dipole–dipole interaction of inter-NPs, the electronic coupling is a short-range process of adjacent NPs. Electronic coupling requires strong inter-NPs interactions and a high degree of structural order (Fig. 3(a)). The individual NPs usually display a discrete electronic state. However, as for strong electronic coupling, extended electronic state could be formed due to the wavefunctions of adjacent NPs overlapping (Fig. 3(b)). As the coupling between NPs increases at shorter inter-NPs distances, the electronic states of the SPs will split to form bands (Fig. 3(c)) [46]. When the electronic coupling of NPs becomes strong enough, the NPs in assemblies could be deemed as atom behaviors in the molecules. Homodimer NPs resemble homonuclear diatomic molecules. For the homonuclear atom in the molecule, when the distance between two atoms is decreased, their wave functions will hybridize to form asymmetric bonding state and anti-symmetric anti-bonding state with the energy difference twice that of the hopping energy [47]. The changed potential energy landscape in the fused dimers results in the hybridization of the building block NPs wave functions and presents multicarrier configurations: biexciton and trion (Figs. 3(d) and 3(e)) [47]. Another pathway to produce strong electronic coupling among NPs is by tunneling and exchange coupling of electrons (Fig. 3(f)) [41]. When insulating linker ligands are replaced with exciton-delocalizing ligands such as phenyldithiocarbamate, the specific ligands strongly mix with band-edge state of NPs and such states decrease the tunneling barrier between NPs, which speed up energy transfer between NPs [48, 49]. The basic characteristic of such ligands is that the frontier molecular orbitals usually lie in energetic resonance with valence or conduction band edges of NPs.

4 Emergent fluorescence behaviors of assemblies

Compared with discrete NPs, the performance of NPs assemblies in this stage is not subject to mathematical statistics but with the hierarchy or specialization of fluorescence. The hierarchy or specialization could be summarized as enhanced specific emission and new emission state related to exciton transition, polarization, intermittency, coherence and number distribution.

4.1 PL blinking

Under continuous excitation, nanostructures fluctuate almost

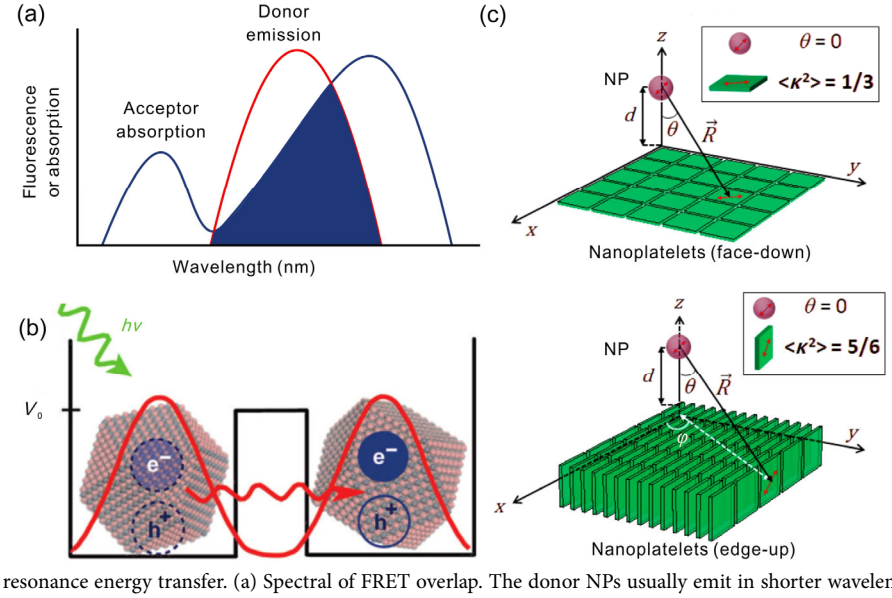

Figure 2 Fluorescence resonance energy transfer. (a) Spectral of FRET overlap. The donor NPs usually emit in shorter wavelengths which overlaps with the acceptor absorption spectrum. (b) FRET is the result of long-distance dipole–dipole interactions between donor and acceptor, but it does not involve the emergence of photons. Reproduced with permission from Ref. [41], © American Chemical Society 2010. (c) Average dipole–dipole interaction coefficient of the NP and the nanoplatelets monolayer with face-down and edge-up orientation. $<\kappa^2>$: the average dipole–dipole interaction coefficient. Reproduced with permission from Ref. [43], © American Chemical Society 2019.

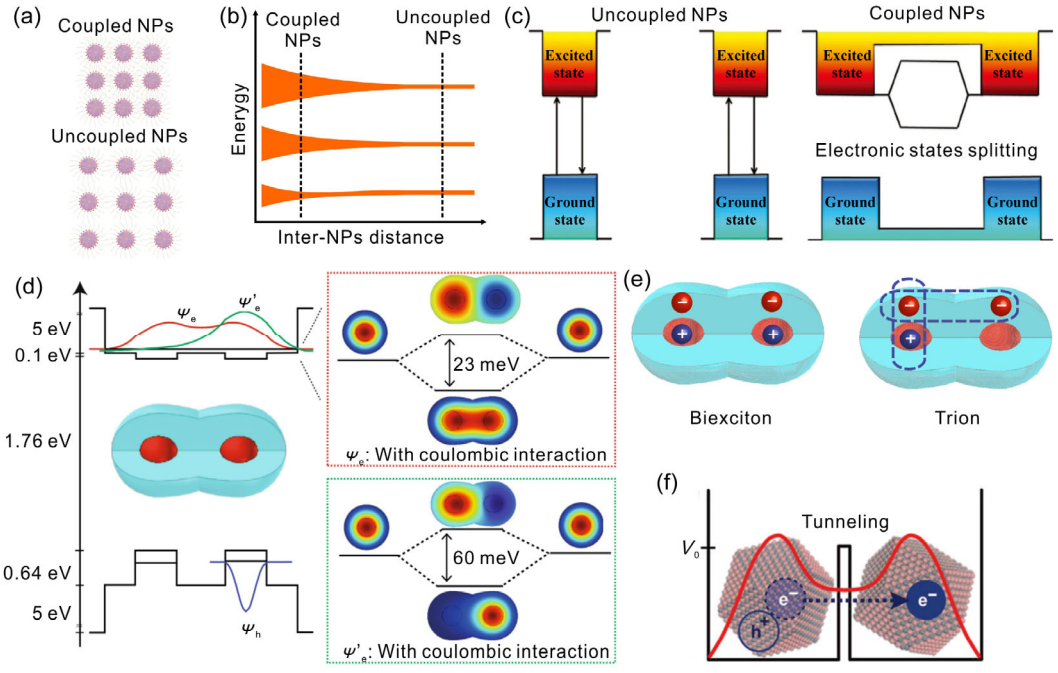

Figure 3 Electronic coupling. (a) Electronic coupling occurs under the short inter-NPs distance in SPs. (b) The electronic state develops gradually from discrete to extended forms as the wavefunctions of neighboring NPs overlap (inter-NPs distance). (c) Energy states of ordered arrays of CdSSe NPs (left) and ordered SPs of CdSSe NPs (right). Due to the sub-nano particle spacing in ordered SPs, NP coupling and new electronic states are generated. Reproduced with permission from Ref. [46], © WILEY-VCH Verlag GmbH & Co. KGaA, Weinheim 2017. (d) The potential energy distribution and cross-section of the first electron wave function without Coulombic interaction (red curve) and with Coulombic interaction (green curve), as well as the hole wave functions (blue curve) of the coupled CdSe/CdS core/shell NPs. Calculated two-dimensional electron wave functions of bonding and anti-bonding without (cross-section is the red region) and with Coulombic interaction (cross-section is the green region). (e) Multicarrier configurations in the coupled CdSe/CdS core/shell NPs molecules. Reproduced with permission from Ref. [47], © Cui, J. B. et al. 2019. (f) Tunneling is also the dominant pathway in the regime of short inter-NPs distance. Reproduced with permission from Ref. [41], © American Chemical Society 2010.

randomly in the PL intensity called blinking. Although the exact mechanism is still under debate, a charging-related Auger recombination is an underlying mechanism to universally explain this blinking [50]. The photophysics of blinking can be viewed as the random switching between on-state (radiative recombination) and off-state (non-radiative Auger recombination), whereby illumination induces charging or ionization (on → off) which is then followed by reneutralization (off → on) [51]. The emission efficiency of the charged state is usually much lower than that of the neutral exciton state. So, the blinking is observed. There are two methods to control blinking fluorescence [52]. One is the elimination of ionization channels in nanostructures to decrease the ratio of the charged state and neutralization state. The elimination of surface defects makes it impossible to capture photogenerated carriers. The other is the improvement of the emission efficiency of charged states. If the non-radiative Auger recombination can be suppressed entirely, the emission efficiency of the charged state will maintain a similar level with the neutral exciton state, and fluctuation of fluorescence intensity versus time will be weakened.

The individual NPs fluorescence intermittency usually exhibits power-law statistical distributions of both the on and off durations [50, 53]. However, fluorescence intermittency of the assemblies of NPs shows distinct behaviors from that of isolated NPs blinking. The coupling effect mainly induces the enhanced transition from dark state to bright states, the increase with "on" times and additional neutral states.

The inter-distance, shape, size difference of adjacent NPs and binary NPs assemblies of electron donor–acceptor have influences on the coupling. Shorter distances of inter-NPs impose more substantial interference of the electronic environment of the neighboring NPs. Yu et al. [54] investigated the CdSe-ZnS NPs and compared individual NPs, small ensembles of isolated NPs (long-distance), and the closed-packed NPs clusters (short distance) by the method of spatially correlated single-molecule fluorescence spectroscopy (Figs. 4(a) and 4(b)). The individual NPs showed the character of prolonged on- and off-blinking times. Multiple isolated NPs also displayed similar independent blinking behavior. However, the fluorescence trajectory of the NPs clusters differs markedly from that of the single NP, which is dominated by extraordinary fast and intense blinking transition as "enhanced" blinking. "Enhanced" blinking could not be suggested to fundamentally generate the collection of individual blinking of multiple NPs. Autocorrelation analysis of the fluorescence trajectories displays that the function of the NP cluster decays precipitously from the minimum lag time [54]. The observed character originates from electronically coupled photoexcited NPs in the cluster. One possible explanation is that an externally trapped electron from off blinking NP in the cluster alters the electronic environment of the neighboring NP, enhancing the fluorescence intensity, a phenomenon analogous to photoinduced fluorescence enhancement, in which a gradual increase of the trapped electrons follows continuous photoexcitation. Compared with well-separated nanorods, the close-packed nanorods shows the enhancement of on-times in fluorescence [55]. The edge-to-edge tunneling might keep at least one of nanorods uncharged and result in stable off-time distribution and extended bright periods. For two tightly packed NPs with small energy gaps, there are four possible on (red) and off (grey) configurations to consider [56]. In situation I, NPs are in the off state and photons are emitted. In situation II, NP1 (the donor) is in the on state and NP2 (the acceptor) is in the off state, leading to low-intensity emission faster than the energy transfer. In

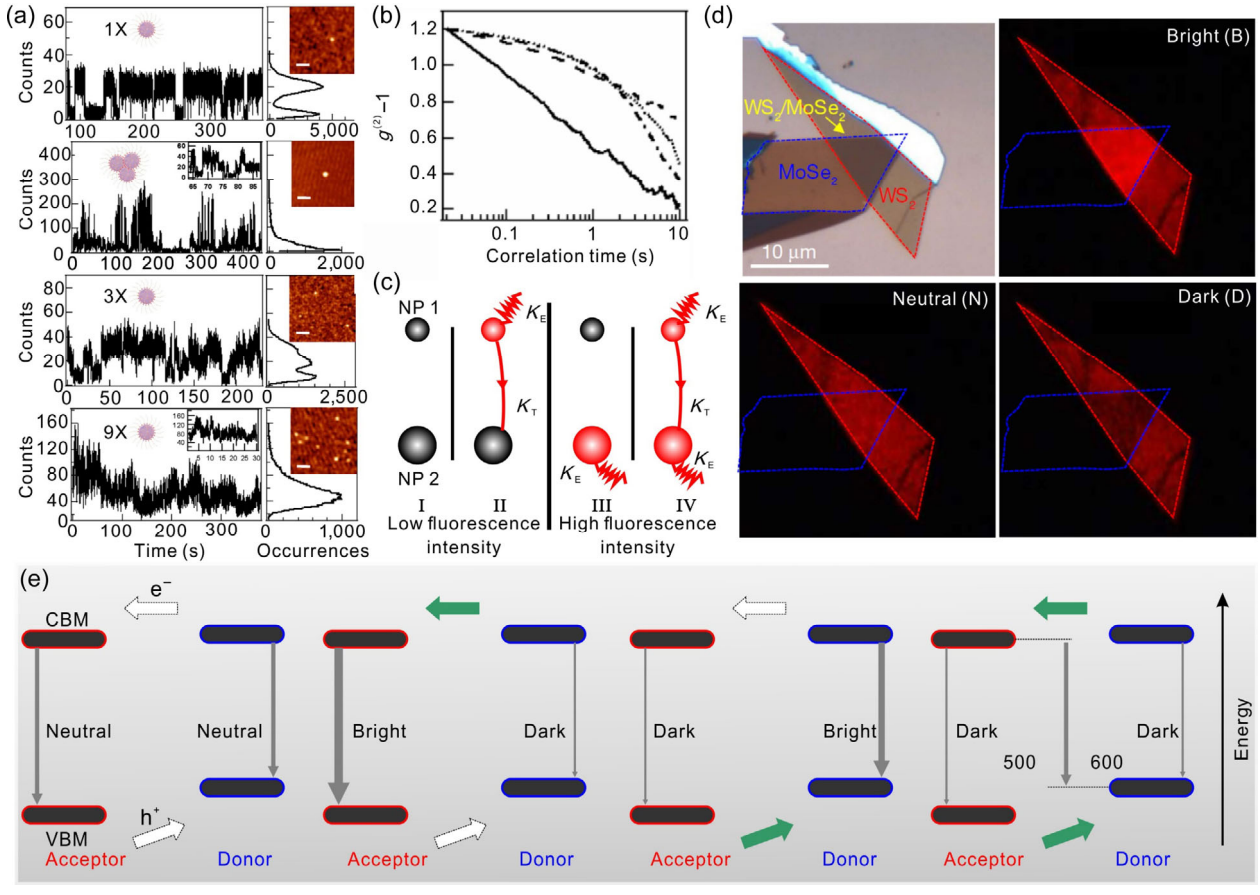

Figure 4 PL blinking. (a) Fluorescence trajectory segments (left) and photon count histograms (right) (insert: AFM topography images of single NP, a NPs cluster, three isolated NPs, and nine isolated NPs respectively probed simultaneously. Scale bars: 98 nm, *z* ranges: 8 nm), (b) Autocorrelation functions of the fluorescence trajectories with the normalization of autocorrelation functions to the same value (single NP: dashed-dotted line, NP cluster: solid line, three isolated NPs: dotted line, multiple isolated NPs: dashed line). Reproduced with permission from Ref. [54], © American Physical Society 2006. (c) The energy transfer kinetics of two tightly packed NPs with different energy gaps are presented. According to the on (orange) or off (gray) status of each NP, four situations need to be considered. Reproduced with permission from Ref. [56], © American Physical Society 2010. (d) The optical image of the trapezoid $WS_2/MoSe_2$ bilayer and the fluorescent images taken by the camera at different times. Reproduced with permission from Ref. [57], © Macmillan Publishers Limited, part of Springer Nature 2017. (e) The intermittent interlayer carrier-transfer model of fluorescence blinking. Band alignment showing the conduction band minimum (CBM) and valence band maximum (VBM) of a typical bilayer heterostructure, with one component acting as an electron donor (for example, $MoSe_2$ in $WS_2/MoSe_2$) and its counterpart as an electron acceptor (for example, WS_2 in $WS_2/MoSe_2$). Grey arrows indicate the emission of an A-exciton from the electron acceptor and the electron donor. e^-, electron; h^+, hole. A neutral state; an electron-dominated carrier-transfer process, which will result in a dark emission state in the electron donor and a bright state in the electron acceptor; a hole-dominated carrier-transfer process, which will result in a bright emission state in the electron donor and a dark state in the electron acceptor; a bilayer heterostructure with unimpeded carrier-transfer channels (for both electrons and holes). Emission from electron donor and acceptor will be quenched.

situation III, the switch state is reversed, resulting in emitting at the featured lifetime and intensity of NP2. In situation IV, both are in the on state, which leads to the mixed emission time and intensity of both NP1 and NP2 due to the energy transfer. In short, the cases I and II feature the majority of low fluorescence intensity and/or rapid fluorescence decay. In contrast, the cases III and IV feature the high-intensity fluorescence and slow fluorescence decay [56]. This simple model displays the coupling state between NPs in a cluster that influences the blinking [56].

When one electron donor NP assemblies with one electron acceptor, inter-NPs carrier transfer process will induce new blinking states (for example, neutral states). Xu et al. [57] designed two monolayers of $WS_2/MoSe_2$ stacked vertically in Lego-like fashion. The bilayers show a correlated blinking emergent effect with bright states in one monolayer and dark states in the other (neutral states). The blinking transforms among bright, neutral and dark states (Figs. 4(d) and 4(e)). The intermittent interlayer carrier-transfer process accounts for the new blinking states.

4.2 Phonon line emission

The PL spectrum of individual NPs generally does not exhibit phonon line emission peaks due to weaker intensity compared to band edge transition. However, in assemblies, the decrease of inter-NPs distance makes it possible for the high efficiency of radiation energy transfer. The inversion of peaks intensity can be achieved by the Stokes-shift-engineering of NPs. For example, the CdSe nanoplatelets exhibited small stokes shift between first exciton absorption and primary PL peaks and their stacked assemblies showed longitudinal optical phonon replica of the band-edge exciton (Fig. 5) [58]. The photons emitted from band edge exciton transition can be efficiently reabsorbed by neighboring nanoplatelets because of the small Stokes shift between the primary peak emission and the first absorption exciton. However, while compared with the primary peak emission, the longitudinal optical phonon replica is red-shifted and it cannot be reabsorbed by a neighboring nanoplatelet. The lateral extension of the stacked nanoplatelets will increase the intensity ratio of phonon line emission and

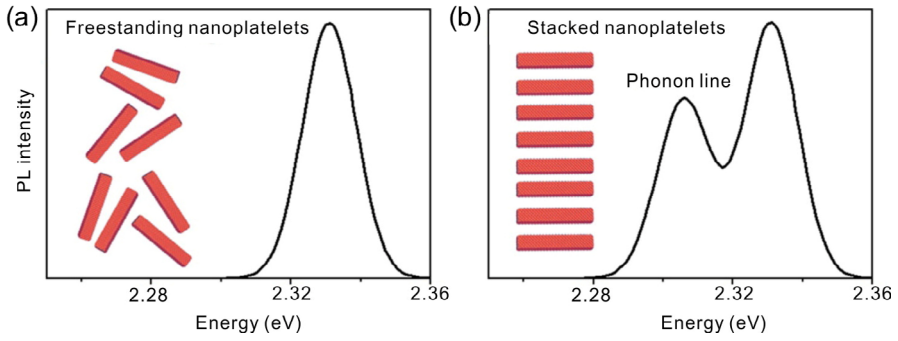

Figure 5 Phonon line emission. Photoluminescence spectra of the solution with non-stacking nanoplatelets (a) and with stacking nanoplatelets (b). There is the phonon line in stacking nanoplatelets. Reproduced with permission from Ref. [58], © American Chemical Society 2013.

edge transition emission because the absorption of the band-edge transition rises with the lateral area—the difference of the radiative energy transfer resulting in intensity variations between the two peaks in self-assembled nanoplates. By designing small stokes shift, low energy phonon replica and high reabsorption efficiency of main band edge transition, assembly of NPs will make it possible to create phonon line emission for light-emitting diodes and laser.

4.3 Linearly polarized luminescence

Photoluminescent anisotropy of low-dimensional matters can be divided into three mechanisms: (1) transition dipole moment alignment (the strength and direction of the electronic oscillation between the ground and emissive states of the emitter), (2) dielectric contrast between the emitter and surrounding environment (mainly excitation field anisotropy) [59, 60], and (3) optical matrix element anisotropy induced by quantum confinement effects [61, 62].

When one component's nanorods are nested in another component's nanorods, the assembled materials exhibit lower polarized emission than the single component rod. For example, highly luminescent CdSe/CdS nanoheterostructures with CdSe rod nested into the CdS rod exhibited a lower emission polarization of 0.82 than that of a single kind of CdSe nanorod (0.85) [63]. However, when such CdSe/CdS nanorods were assembled into needle-like single-domain superstructures embedded in polydimethylsiloxane (PDMS) films, an emission polarization factor of up to 0.88 could be achieved (Figs. 6(a)–6(c)) [64]. The linear polarization ratio is higher than 0.75 of isolated single CdSe-CdS nanorods with a similar aspect ratio [63, 65]. This PL polarization enhancement is supposed to benefit from second-order synergistic complementarity of the superstructures [6]. Due to the isotropic nature of quantum dots, it is generally considered that quantum dots do not exhibit polarized emission. When quantum dots are well aligned into the chain, the wire-shape position order structure along the alignment direction of quantum dots usually displays high linear polarization. Embedding the laterally ordered InP quantum dots into an $In_{0.48}Ga_{0.52}P$ matrix showed a polarization degree of 0.66 (Figs. 6(d) and 6(e)) [66]. Compared to the building blocks, this may be attributed to the increased aspect ratio of the whole assemblies.

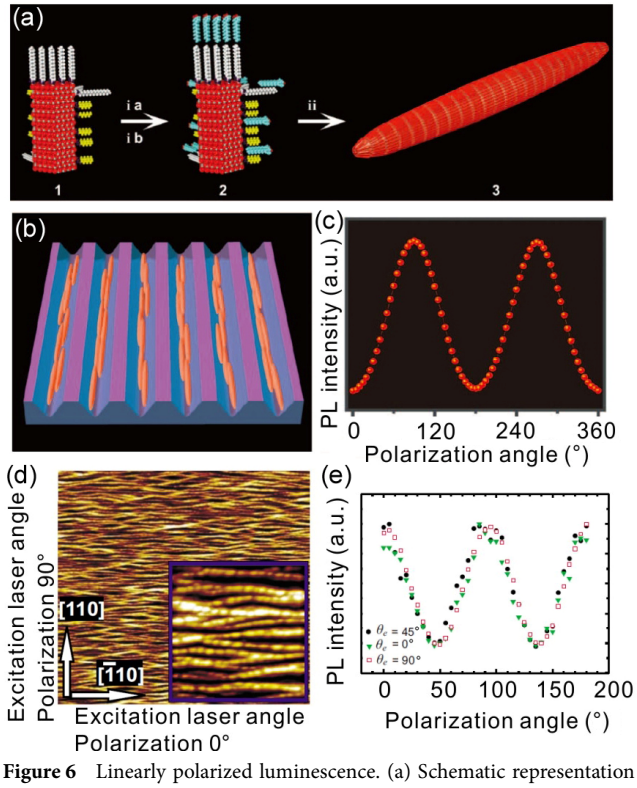

Figure 6 Linearly polarized luminescence. (a) Schematic representation for the synthesis of needle-like superparticle. (b) Graphic representation of the transverse alignment of superparticles on a solid substrate. (c) The relationship between the PL intensity and the polarization angle of typical superparticles embedded PDMS film at the excitation wavelength of 380 nm. Reproduced with permission from Ref. [64], © American Association for the Advancement of Science 2012. (d) Atomic force microscopy (AFM) micrograph of the laterally ordered InP quantum dots into an $In_{0.48}Ga_{0.52}P$ matrix without a cap layer with excitation directions. (e) Polarization-dependent PL spectra of packed InP quantum dots. Reproduced with permission from Ref. [66], © American Institute of Physics 2010.

4.4 Circularly polarized luminescence

Circularly polarized luminescence is a phenomenon that the chiral system emits the photon with preferential left-handed or right-handed rotating vector at a circular frequency ω. The optical activity of the semiconductor NPs such as CdS and CdTe quantum dots, usually originates from the surface chiral molecules [67]. Circularly polarized luminescence or circular dichroism intensity could be modified by the alternation of size, shape, composition and crystal structure. Assembly provides the additional possible method to enhance or break the original rotational symmetry by chiral transfer or a specific chiral arrangement in spatial position.

The energy transfer from a chiral donor to an achiral acceptor is a proven pathway to improve circularly polarized luminescence of the assemblies. When CdSe/ZnS core–shell NPs are well-ordered assembled onto the chiral tubular lipid gelator by the electrostatic interaction between carboxylate groups of surface achiral 3-mercaptopropionic acid of NPs and the amine groups of the gelator, the circularly polarized luminescence could be observed (Fig. 7(a)) [68]. However, the mixture exhibited no

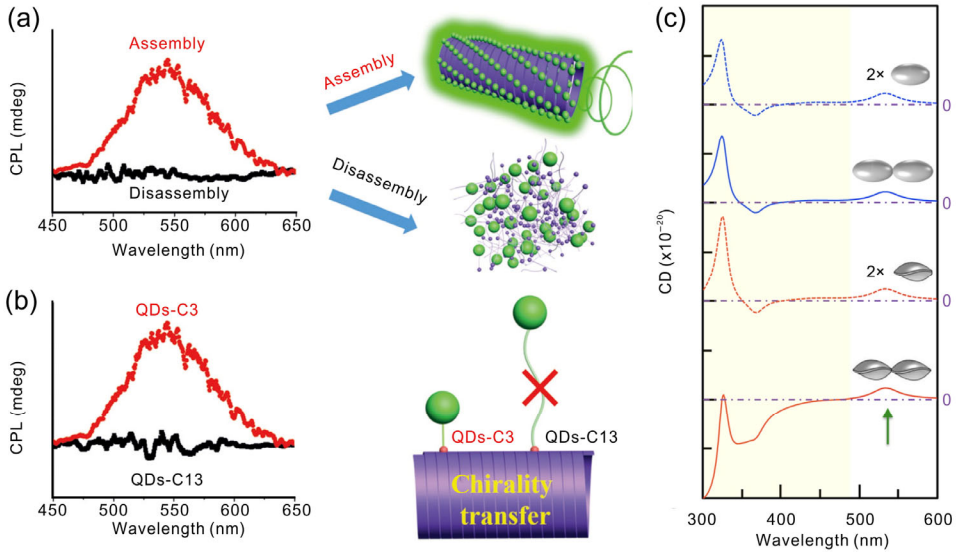

Figure 7 Circularly polarized luminescence. (a) CPL spectra of CdSe/ZnS NP doped co-gels in assembled and disassembled states. (b) CPL spectra of NPs with different interval lengths of the capping reagent. Reproduced with permission from Ref. [68], © WILEY-VCH Verlag GmbH & Co. KGaA, Weinheim 2017. (c) Evolution of CD curves in the assembled α-HgS chain with two different building blocks. Reproduced with permission from Ref. [71], © American Chemical Society 2017.

circularly polarized luminescence. If the spacer between carboxylic acid and thiol on the surface of the NPs is too large, it is hard to produce circularly polarized luminescence (Fig. 7(b)). The hydrogen bonding, electrostatic interaction and weak π–π interaction between a chiral donor and an achiral acceptor might be the best choice to realize the energy transfer.

Circularly polarized luminescence of the assemblies induced by the chiral structural adjustment of the assembly of achiral NPs will open up a new door to create the circularly polarized luminescence active materials. However, it remains a huge challenge for NPs assemblies. The concepts of creating the circularly polarized luminescence from chiral spiral structural molecular assemblies have already been proven by vortex mixing in the assembly process [69, 70]. Perhaps, chiral spiral structural adjustment of the assembly of NPs is a potential strategy. Additionally, co-assembly of luminescent NPs and magnetic NPs might be one general strategy for applying the magnetic field along the direction of excitation or emission of chiral aligned luminescent NPs to control the circularly polarized luminescence.

The shape of NPs will also determine the expression of chirality. In general, the coupling of chiral α-HgS nanoellipsoids shows virtually no difference in the sum circular dichroism (CD) signal among two individual nanoellipsoids [71]. However, a chain superstructure consisting of two left-twisted bipyramids manifests significant modification of their chiroptical response under 500 nm (Fig. 7(c)) [71]. This could be induced by periodic morphology-enhanced chiral coupling by the assembly [71].

4.5 Superfluorescence

When individual building blocks of emitter interact coherently via a fluorescence radiation field, the assembly exhibits coherent spontaneous emission that consists of two types of emission: superradiance (SR) or superfluorescence (SF). Both SR and SF are emergent emissions arising from a total population inversion initially formed by an initially incoherent ensemble into a dense coherent ensemble. If a dense population inversion was induced coherently by a laser field due to macroscopic polarization, the resultant emission is SR. As for SF, spontaneous coherence over a subset of excited states can be formed from an initially incoherent dense population inversion with a unique featured induction time τ_D. The emission was first pointed out against that individual molecule emitting a photon usually is independent of the states of other molecules by Dicke in 1954 [72]. The spontaneous emission of an excited state is usually considered as a random process where the stored energy is released within the natural lifetime τ_n of the excited state. However, as for SR and SF, the stored energy is released within a shorter time (τ_n/N, where N is the number of excited atoms). Moreover, the emission intensity is proportional to N^2 instead of N [73]. The prediction is no doubt that emergent behavior develops in this system.

Rainò et al. [74] showed that self-assembly superlattices from cesium lead halide perovskite NPs exhibited superfluorescence behavior beyond individual nanocrystal (Fig. 8). The observed distinct SF characteristics are proved by the absence of dynamic red-shift of emission, accelerated radiative decay and the extension of the first-order coherence time by more than a factor of four, photon bunching, as well as delayed emission pulses with Burnham-Chiao ringing behavior in the time domain at high excitation density. However, uncoupled NPs dispersed in polystyrene were tested under similar excitation conditions and displayed no of the above-mentioned signatures of SF.

4.6 Photon antibunching

The photon bunching phenomenon is that the photons of emitter are in the form of clusters or bunches spacing, which is a property of the incoherent or chaotic light from conventional

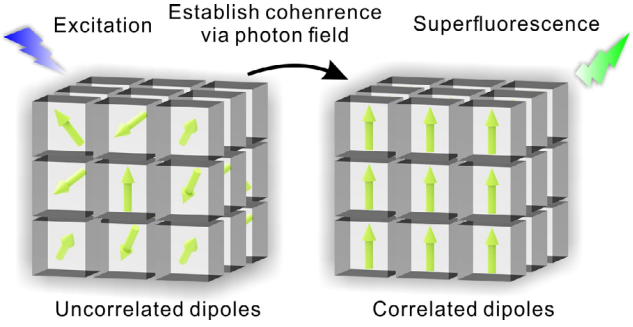

Figure 8 Schematic diagram of superfluorescence formation process of a single $CsPbBr_3$ nanocube superlattice.

thermal light field sources [75]. The antibunching is a sub-Poissonian characteristic of light, which is a photon number distribution with a variance less than the mean (Fig. 9(a)). The ideal process is that only one single exciton left in the emitter emits a photon. To obtain antibunching photons of matters, it is usually necessary to suppress the emission efficiency of multiple excitons by improving Auger efficiency. For assemblies, photon antibunching is a nonlinear correlation with the number of NPs increasing. For example, single CdSe/CdS core/shell monomers usually showed strong photon antibunching (Fig. 9(b)) [47]. In comparison, fused dimers exhibited low Auger decay and low antibunching contrast (Fig. 9(c)). However, the collective fluorescent photons emitted by a cluster of four giant CdSe/CdS NPs at 4 K displayed a $g^{(2)}$ value less than 0.15 at the zero-time delay, which implies strong Auger decay and photon antibunching effect (Figs. 9(d) and 9(e)) [76]. When the number of NPs increases from one to four, photon antibunching shows a concave trend, which might imply Auger efficiency and multiexciton configurations of quantitative correlation. It requires more experimental measurements and theoretical treatments further to understand the physical mechanism of nonlinear antibunching in assemblies.

5 Conclusions and outlook

At each level of complexity entirely new properties appear [6]. Studies on the new type of fluorescent properties of assemblies and their exclusive concepts are still in its infancy. In this review, we propose the concepts of emergent behaviors of assemblies and highlight the relationship between the coupling of inter-NPs and induced fluorescent properties of assemblies. A few examples of exciton transition, polarization, intermittency, coherence and number distribution in the coupling are then presented. Besides, the design of coupling processes, including radiative energy transfer, fluorescence resonance energy transfer and electronic coupling, is critical for building emergent behaviors. Herein, we formulate three main directions or initiatives

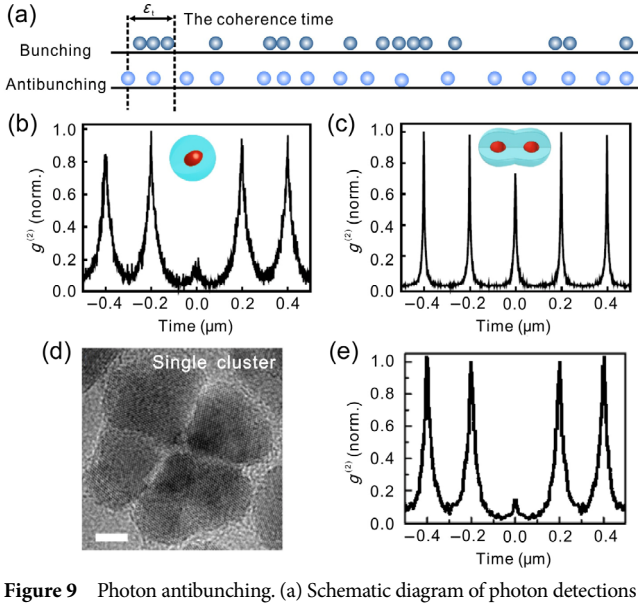

Figure 9 Photon antibunching. (a) Schematic diagram of photon detections as a function of bunching and antibunching time. ε_t is the coherence time. (b) Second-order photon correlation measurement for single CdSe/CdS core/shell NP. (c) Second-order photon correlation measurement for fused CdSe/CdS core/shell NPs dimer. Reproduced with permission from Ref. [47], © Cui, J. B. et al. 2019. (d) High-resolution transmission electron microscopy (TEM) images of single CdSe/CdS cluster. (e) Second-order photon correlation measurement for single CdSe/CdS cluster. Reproduced with permission from Ref. [76], © Lv, B. H. et al. 2018.

where enormous progress is made on answering the essential question of "more is different."

First, the fundamental understanding and regulation of the coupling behaviors of NPs in assemblies or superstructures call for further development. Strategies for constructing emergent behaviors are only true in specific assemblies, but whether the strategies are the common ways is still unknown. The inherent and generalized physical and chemical relationships between coupling and fluorescence behaviors shall be established and studied. The coupling is the function of the distance of inter-NPs, but questions are often raised, such as, "how many is the critical distance to induce the transformation of specific fluorescence behavior?" and "how to predict the critical distance in different assemblies?" The periodic table of the coupling characteristic distances of different NPs needs to be established by experiments and simulations. It should also be stressed that the precise distance control is a system engineering, which demands the systematic design of element, shape, size and crystal structure of NPs, specific facets or surface atoms, ligand type and length. The alignment of the transition dipole caused by the shape of NPs and orientation of atoms will widen the possibilities to create novel coupling.

Second, when the arrangement of NPs evolves from short-term to the long-term order, specific patterns or phase structures are formed and the coupling between inter-NPs begins to transform into the emergent behaviors induced by phase behavior. The symmetry breaking at the microscale level in the same magnitude as light wavelength due to the pattern formation of NPs in assemblies, modulates the photon state, which is different from the modulation of single NP. The relationships between the phase structure of assemblies and the induced emergent fluorescent behavior are still unclear. Akin to any solid, assemblies can contain more than one type of structural defect in positioning the building blocks, including point defects, line defects, planar defects, and volume defects. However, how these affect fluorescence evolution has not been reported and there is no model to predict the trend. Similar to the conformation in polymers, the positioning and orientation of specific building blocks in assemblies shall also be examined to induce the generation of the emergent fluorescence. Furthermore, it also imposes higher requirements for developing the new self-assembly techniques to precisely control the assemblies or superstructure on multiscale position ordering or defects from the atomic scale to the centimeter scale.

Finally, the assemblies of various types of building blocks may have the effect of multiplying or dividing properties among constituents. The assemblies could be the complex system consisting of P-type/N-type semiconductor, isotropic/anisotropic shape, singlet/triplets emission, or high/low refractive index structures and show cooperative complementary coupling processes. Besides NPs, functional molecules as linkers or ligand of NPs such as delayed fluorescence molecules, pH-responsive molecules, pressure-responsive molecules and temperature-responsive molecules also play the important roles on the coupling-emergent behavior. Therefore, the accumulation of knowledge regarding the coupling of binary and diversified assemblies will lead to new insights into emergent behaviors.

The exploration of emergent behaviors on the fluorescence of self-assembly will serve as a bridge between fundamental researches and optical-based devices and facilitate the next generation of optical applications. Considering the similar hierarchical functional deployment caused by self-assembly in biology, electricity, magnetism, acoustics and mechanics, methodological cognition in accumulations of the realization of emergent fluorescence properties from NPs to assemblies

will also be significant for understanding other self-assembly functional expression processes.

Acknowledgements

This work was financially supported by the National Natural Science Foundation of China (Nos. 21925405 and 201874005), the National Key Research and Development Program of China (No. 2018YFA0208800), and Chinese Academy of Sciences (Nos. XDA23030106 and YJKYYQ20180044).

References

[1] Kagan, C. R.; Murray, C. B. Charge transport in strongly coupled quantum dot solids. *Nat. Nanotechnol.* **2015**, *10*, 1013–1026.

[2] Liu, C.; Zheng, L. R.; Song, Q.; Xue, Z. J.; Huang, C. H.; Liu, L.; Qiao, X. Z.; Li, X.; Liu, K. Y.; Wang, T. A metastable crystalline phase in two-dimensional metallic oxide nanoplates. *Angew. Chem., Int. Ed.* **2019**, *58*, 2055–2059.

[3] Liu, Y. X.; Vanacken, J.; Chen, X. M.; Han, J. B.; Zhong, Z. Q.; Xia, Z. C.; Chen, B. R.; Wu, H.; Jin, Z.; Ge, J. Y. et al. Direct observation of nanoscale light confinement without metal. *Adv. Mater.* **2019**, *31*, 1806341.

[4] Xue, Z. J.; Yan, C.; Wang, T. From atoms to lives: The evolution of nanoparticle assemblies. *Adv. Funct. Mater.* **2019**, *29*, 1807658.

[5] Zhang, H.; Li, H. Y.; Akram, B.; Wang, X. Fabrication of NiFe layered double hydroxide with well-defined laminar superstructure as highly efficient oxygen evolution electrocatalysts. *Nano Res.* **2019**, *12*, 1327–1331.

[6] Yan, C.; Wang, T. A new view for nanoparticle assemblies: From crystalline to binary cooperative complementarity. *Chem. Soc. Rev.* **2017**, *46*, 1483–1509.

[7] Yang, B.; Zhou, S.; Zeng, J.; Zhang, L. P.; Zhang, R. H.; Liang, K.; Xie, L.; Shao, B.; Song, S. L.; Huang, G. et al. Super-assembled core-shell mesoporous silica-metal-phenolic network nanoparticles for combinatorial photothermal therapy and chemotherapy. *Nano Res.* **2020**, *13*, 1013–1019.

[8] Qiao, X. Z.; Chen, X. Y.; Huang, C. H.; Li, A. L.; Li, X.; Lu, Z. L.; Wang, T. Detection of exhaled volatile organic compounds improved by hollow nanocages of layered double hydroxide on Ag nanowires. *Angew. Chem., Int. Ed.* **2019**, *58*, 16523–16527.

[9] Qin, X. Y.; Wang, T.; Jiang, L. Surface engineering of nanoparticles for triggering collective properties of supercrystals. *Natl. Sci. Rev.* **2017**, *4*, 672–677.

[10] Zhao, X.; Zha, X. J.; Tang, L. S.; Pu, J. H.; Ke, K.; Bao, R. Y.; Liu, Z. Y.; Yang, M. B.; Yang, W. Self-assembled core-shell polydopamine@MXene with synergistic solar absorption capability for highly efficient solar-to-vapor generation. *Nano Res.* **2020**, *13*, 255–264.

[11] Anderson, P. W. More is different. *Science* **1972**, *177*, 393–396.

[12] Martynenko, I. V.; Baimuratov, A. S.; Weigert, F.; Soares, J. X.; Dhamo, L.; Nickl, P.; Doerfel, I.; Pauli, J.; Rukhlenko, I. D.; Baranov, A. V. et al. Photoluminescence of Ag-In-S/ZnS quantum dots: Excitation energy dependence and low-energy electronic structure. *Nano Res.* **2019**, *12*, 1595–1603.

[13] Bischof, T. S.; Correa, R. E.; Rosenberg, D.; Dauler, E. A.; Bawendi, M. G. Measurement of emission lifetime dynamics and biexciton emission quantum yield of individual InAs colloidal nanocrystals. *Nano Lett.* **2014**, *14*, 6787–6791.

[14] Hughes, K. E.; Stein, J. L.; Friedfeld, M. R.; Cossairt, B. M.; Gamelin, D. R. Effects of surface chemistry on the photophysics of colloidal InP nanocrystals. *ACS Nano* **2019**, *13*, 14198–14207.

[15] Lv, Y.; Huang, X. N.; Zhang, C. F.; Wang, X. Y.; Xiao, M. Multiple dark excitons in semiconductor CdSe nanocrystals. *J. Phys. Chem. C* **2018**, *122*, 23758–23763.

[16] Becker, M. A.; Vaxenburg, R.; Nedelcu, G.; Sercel, P. C.; Shabaev, A.; Mehl, M. J.; Michopoulos, J. G.; Lambrakos, S. G.; Bernstein, N.; Lyons, J. L. et al. Bright triplet excitons in caesium lead halide perovskites. *Nature* **2018**, *553*, 189–193.

[17] Tamarat, P.; Bodnarchuk, M. I.; Trebbia, J. B.; Erni, R.; Kovalenko, M. V.; Even, J.; Lounis, B. The ground exciton state of formamidinium lead bromide perovskite nanocrystals is a singlet dark state. *Nat. Mater.* **2019**, *18*, 717–724.

[18] Sichert, J. A.; Tong, Y.; Mutz, N.; Vollmer, M.; Fischer, S.; Milowska, K. Z.; García Cortadella, R.; Nickel, B.; Cardenas-Daw, C.; Stolarczyk, J. K. et al. Quantum size effect in organometal halide perovskite nanoplatelets. *Nano Lett.* **2015**, *15*, 6521–6527.

[19] Lin, S. X.; Li, J. Z.; Pu, C. D.; Lei, H. R.; Zhu, M. Y.; Qin, H. Y.; Peng, X. G. Surface and intrinsic contributions to extinction properties of ZnSe quantum dots. *Nano Res.* **2020**, *13*, 824–831.

[20] Brus, L. Electronic wave functions in semiconductor clusters: Experiment and theory. *J. Phys. Chem.* **1986**, *90*, 2555–2560.

[21] Kim, Y.; Ham, S.; Jang, H.; Min, J. H.; Chung, H.; Lee, J.; Kim, D.; Jang, E. Bright and uniform green light emitting InP/ZnSe/ZnS quantum dots for wide color gamut displays. *ACS Appl. Nano Mater.* **2019**, *2*, 1496–1504.

[22] Xu, Z. H.; Li, Y.; Li, J. Z.; Pu, C. D.; Zhou, J. H.; Lv, L. L.; Peng, X. G. Formation of size-tunable and nearly monodisperse InP nanocrystals: Chemical reactions and controlled synthesis. *Chem. Mater.* **2019**, *31*, 5331–5341.

[23] Boles, M. A.; Ling, D. S.; Hyeon, T.; Talapin, D. V. The surface science of nanocrystals. *Nat. Mater.* **2016**, *15*, 141–153.

[24] Han, P. G.; Zhang, X.; Mao, X.; Yang, B.; Yang, S. Q.; Feng, Z. C.; Wei, D. H.; Deng, W. Q.; Pullerits, T.; Han, K. L. Size effect of lead-free halide double perovskite on luminescence property. *Sci. China Chem.* **2019**, *62*, 1405–1413.

[25] Gao, Y.; Peng, X. G. Photogenerated excitons in plain core CdSe nanocrystals with unity radiative decay in single channel: The effects of surface and ligands. *J. Am. Chem. Soc.* **2015**, *137*, 4230–4235.

[26] Li, X.; Xue, Z. J.; Luo, D.; Huang, C. H.; Liu, L. Z.; Qiao, X. Z.; Liu, C.; Song, Q.; Yan, C.; Li, Y. C. et al. A stable lead halide perovskite nanocrystals protected by PMMA. *Sci. China Mater.* **2018**, *61*, 363–370.

[27] Li, X. C.; Li, C. L.; Wu, Y. Y.; Cao, J.; Tang, Y. A reaction-and-assembly approach using monoamine zinc porphyrin for highly stable large-area perovskite solar cells. *Sci. China Chem.* **2020**, *63*, 777–784.

[28] Jasieniak, J.; Mulvaney, P. From Cd-rich to Se-rich—The manipulation of CdSe nanocrystal surface stoichiometry. *J. Am. Chem. Soc.* **2007**, *129*, 2841–2848.

[29] Rempel, J. Y.; Trout, B. L.; Bawendi, M. G.; Jensen, K. F. Density functional theory study of ligand binding on CdSe (0001), (000$\bar{1}$), and (11$\bar{2}$0) single crystal relaxed and reconstructed surfaces: Implications for nanocrystalline growth. *J. Phys. Chem. B* **2006**, *110*, 18007–18016.

[30] Zherebetskyy, D.; Scheele, M.; Zhang, Y. J.; Bronstein, N.; Thompson, C.; Britt, D.; Salmeron, M.; Alivisatos, P.; Wang, L. W. Hydroxylation of the surface of PbS nanocrystals passivated with oleic acid. *Science* **2014**, *344*, 1380–1384.

[31] Aldana, J.; Wang, Y. A.; Peng, X. G. Photochemical instability of CdSe nanocrystals coated by hydrophilic thiols. *J. Am. Chem. Soc.* **2001**, *123*, 8844–8850.

[32] Thompson, N. J.; Wilson, M. W. B.; Congreve, D. N.; Brown, P. R.; Scherer, J. M.; Bischof, T. S.; Wu, M. F.; Geva, N.; Welborn, M.; Van Voorhis, T. et al. Energy harvesting of non-emissive triplet excitons in tetracene by emissive PbS nanocrystals. *Nat. Mater.* **2014**, *13*, 1039–1043.

[33] Tabachnyk, M.; Ehrler, B.; Gélinas, S.; Böhm, M. L.; Walker, B. J.; Musselman, K. P.; Greenham, N. C.; Friend, R. H.; Rao, A. Resonant energy transfer of triplet excitons from pentacene to PbSe nanocrystals. *Nat. Mater.* **2014**, *13*, 1033–1038.

[34] Mongin, C.; Garakyaraghi, S.; Razgoniaeva, N.; Zamkov, M.; Castellano, F. N. Direct observation of triplet energy transfer from semiconductor nanocrystals. *Science* **2016**, *351*, 369–372.

[35] Wu, M. F.; Congreve, D. N.; Wilson, M. W. B.; Jean, J.; Geva, N.; Welborn, M.; Van Voorhis, T.; Bulović, V.; Bawendi, M. G.; Baldo, M. A. Solid-state infrared-to-visible upconversion sensitized by colloidal nanocrystals. *Nat. Photonics* **2016**, *10*, 31–34.

[36] Mongin, C.; Moroz, P.; Zamkov, M.; Castellano, F. N. Thermally activated delayed photoluminescence from pyrenyl-functionalized CdSe quantum dots. *Nat. Chem.* **2018**, *10*, 225–230.

[37] Fang, Z. W.; Xing, Q. Y.; Fernandez, D.; Zhang, X.; Yu, G. H. A mini review on two-dimensional nanomaterial assembly. *Nano Res.* **2020**, *13*, 1179–1190.

[38] Nguyen, H. M.; Seitz, O.; Peng, W. N.; Gartstein, Y. N.; Chabal, Y. J.; Malko, A. V. Efficient radiative and nonradiative energy transfer from proximal CdSe/ZnS nanocrystals into silicon nanomembranes. *ACS Nano* **2012**, *6*, 5574–5582.
[39] Meinardi, F.; Colombo, A.; Velizhanin, K. A.; Simonutti, R.; Lorenzon, M.; Beverina, L.; Viswanatha, R.; Klimov, V. I.; Brovelli, S. Large-area luminescent solar concentrators based on "stokes-shift-engineered" nanocrystals in a mass-polymerized PMMA matrix. *Nat. Photonics* **2014**, *8*, 392–399.
[40] Li, Z. L.; Johnston, A.; Wei, M. Y.; Saidaminov, M. I.; Martins de Pina, J.; Zheng, X. P.; Liu, J. K.; Liu, Y.; Bakr, O. M.; Sargent, E. H. Solvent-solute coordination engineering for efficient perovskite luminescent solar concentrators. *Joule* **2020**, *4*, 631–643.
[41] Choi, J. J.; Luria, J.; Hyun, B. R.; Bartnik, A. C.; Sun, L. F.; Lim, Y. F.; Marohn, J. A.; Wise, F. W.; Hanrath, T. Photogenerated exciton dissociation in highly coupled lead salt nanocrystal assemblies. *Nano Lett.* **2010**, *10*, 1805–1811.
[42] Curutchet, C.; Franceschetti, A.; Zunger, A.; Scholes, G. D. Examining förster energy transfer for semiconductor nanocrystalline quantum dot donors and acceptors. *J. Phys. Chem. C* **2008**, *112*, 13336–13341.
[43] Erdem, O.; Gungor, K.; Guzelturk, B.; Tanriover, I.; Sak, M.; Olutas, M.; Dede, D.; Kelestemur, Y.; Demir, H. V. Orientation-controlled nonradiative energy transfer to colloidal nanoplatelets: Engineering dipole orientation factor. *Nano Lett.* **2019**, *19*, 4297–4305.
[44] Shen, Y. Z.; Sun, Y. D.; Yan, R. Q.; Chen, E. Q.; Wang, H.; Ye, D. J.; Xu, J. J.; Chen, H. Y. Rational engineering of semiconductor QDs enabling remarkable $^1O_2$ production for tumor-targeted photodynamic therapy. *Biomaterials* **2017**, *148*, 31–40.
[45] Shen, Y. Z.; Tian, Q.; Sun, Y. D.; Xu, J. J.; Ye, D. J.; Chen, H. Y. ATP-activatable photosensitizer enables dual fluorescence imaging and targeted photodynamic therapy of tumor. *Anal. Chem.* **2017**, *89*, 13610–13617.
[46] Luo, D.; Qin, X. Y.; Song, Q.; Qiao, X. Z.; Zhang, Z.; Xue, Z. J.; Liu, C.; Mo, G.; Wang, T. Ordered superparticles with an enhanced photoelectric effect by sub-nanometer interparticle distance. *Adv. Funct. Mater.* **2017**, *27*, 1701982.
[47] Cui, J. B.; Panfil, Y. E.; Koley, S.; Shamalia, D.; Waiskopf, N.; Remennik, S.; Popov, I.; Oded, M.; Banin, U. Colloidal quantum dot molecules manifesting quantum coupling at room temperature. *Nat. Commun.* **2019**, *10*, 5401.
[48] Azzaro, M. S.; Dodin, A.; Zhang, D. Y.; Willard, A. P.; Roberts, S. T. Exciton-delocalizing ligands can speed up energy migration in nanocrystal solids. *Nano Lett.* **2018**, *18*, 3259–3270.
[49] Moroz, P.; Royo Romero, L.; Zamkov, M. Colloidal semiconductor nanocrystals in energy transfer reactions. *Chem. Commun.* **2019**, *55*, 3033–3048.
[50] Busov, V. K.; Frantsuzov, P. A. Models of semiconductor quantum dots blinking based on spectral diffusion. *Opt. Spectrosc.* **2019**, *126*, 70–82.
[51] Efros, A. L.; Nesbitt, D. J. Origin and control of blinking in quantum dots. *Nat. Nanotechnol.* **2016**, *11*, 661–671.
[52] Yuan, G. C.; Gómez, D. E.; Kirkwood, N.; Boldt, K.; Mulvaney, P. Two mechanisms determine quantum dot blinking. *ACS Nano* **2018**, *12*, 3397–3405.
[53] Chung, I.; Bawendi, M. G. Relationship between single quantum-dot intermittency and fluorescence intensity decays from collections of dots. *Phys. Rev. B* **2004**, *70*, 165304.
[54] Yu, M.; Van Orden, A. Enhanced fluorescence intermittency of CdSe-ZnS quantum-dot clusters. *Phys. Rev. Lett.* **2006**, *97*, 237402.
[55] Wang, S. Y.; Querner, C.; Dadosh, T.; Crouch, C. H.; Novikov, D. S.; Drndic, M. Collective fluorescence enhancement in nanoparticle clusters. *Nat. Commun.* **2011**, *2*, 364.
[56] Shepherd, D. P.; Whitcomb, K. J.; Milligan, K. K.; Goodwin, P. M.; Gelfand, M. P.; Van Orden, A. Fluorescence intermittency and energy transfer in small clusters of semiconductor quantum dots. *J. Phys. Chem. C* **2010**, *114*, 14831–14837.
[57] Xu, W. G.; Liu, W. W.; Schmidt, J. F.; Zhao, W. J.; Lu, X.; Raab, T.; Diederichs, C.; Gao, W. B.; Seletskiy, D. V.; Xiong, Q. H. Correlated fluorescence blinking in two-dimensional semiconductor heterostructures. *Nature* **2017**, *541*, 62–67.
[58] Tessier, M. D.; Biadala, L.; Bouet, C.; Ithurria, S.; Abecassis, B.; Dubertret, B. Phonon line emission revealed by self-assembly of colloidal nanoplatelets. *ACS Nano* **2013**, *7*, 3332–3340.
[59] Wang, J. F.; Gudiksen, M. S.; Duan, X. F.; Cui, Y.; Lieber, C. M. Highly polarized photoluminescence and photodetection from single indium phosphide nanowires. *Science* **2001**, *293*, 1455–1457.
[60] Kovalev, D.; Ben Chorin, M.; Diener, J.; Koch, F.; Efros, A. L.; Rosen, M.; Gippius, N. A.; Tikhodeev, S. G. Porous Si anisotropy from photoluminescence polarization. *Appl. Phys. Lett.* **1995**, *67*, 1585–1587.
[61] Hu, J. T.; Li, L. S.; Yang, W. D.; Manna, L.; Wang, L. W.; Alivisatos, A. P. Linearly polarized emission from colloidal semiconductor quantum rods. *Science* **2001**, *292*, 2060–2063.
[62] Yamaguchi, A. A. Anisotropic optical matrix elements in strained GaN quantum wells on semipolar and nonpolar substrates. *Jpn. J. Appl. Phys.* **2007**, *46*, L789.
[63] Sitt, A.; Salant, A.; Menagen, G.; Banin, U. Highly emissive nano rod-in-rod heterostructures with strong linear polarization. *Nano Lett.* **2011**, *11*, 2054–2060.
[64] Wang, T.; Zhuang, J. Q.; Lynch, J.; Chen, O.; Wang, Z. L.; Wang, X. R.; LaMontagne, D.; Wu, H. M.; Wang, Z. W.; Cao, Y. C. Self-assembled colloidal superparticles from nanorods. *Science* **2012**, *338*, 358–363.
[65] Talapin, D. V.; Koeppe, R.; Götzinger, S.; Kornowski, A.; Lupton, J. M.; Rogach, A. L.; Benson, O.; Feldmann, J.; Weller, H. Highly emissive colloidal CdSe/CdS heterostructures of mixed dimensionality. *Nano Lett.* **2003**, *3*, 1677–1681.
[66] Ugur, A.; Hatami, F.; Vamivakas, A. N.; Lombez, L.; Atatüre, M.; Volz, K.; Masselink, W. T. Highly polarized self-assembled chains of single layer InP/(In,Ga)P quantum dots. *Appl. Phys. Lett.* **2010**, *97*, 253113.
[67] Gao, X. Q.; Han, B.; Yang, X. K.; Tang, Z. Y. Perspective of chiral colloidal semiconductor nanocrystals: Opportunity and challenge. *J. Am. Chem. Soc.* **2019**, *141*, 13700–13707.
[68] Huo, S. W.; Duan, P. F.; Jiao, T. F.; Peng, Q. M.; Liu, M. H. Self-assembled luminescent quantum dots to generate full-color and white circularly polarized light. *Angew. Chem., Int. Ed.* **2017**, *56*, 12174–12178.
[69] Sang, Y. T.; Han, J. L.; Zhao, T. H.; Duan, P. F.; Liu, M. H. Circularly polarized luminescence in nanoassemblies: Generation, amplification, and application. *Adv. Mater.*, in press, DOI: 10.1002/adma.201900110.
[70] Sang, Y. T.; Yang, D.; Duan, P. F.; Liu, M. H. Towards homochiral supramolecular entities from achiral molecules by vortex mixing-accompanied self-assembly. *Chem. Sci.* **2019**, *10*, 2718–2724.
[71] Wang, P. P.; Yu, S. J.; Ouyang, M. Assembled suprastructures of inorganic chiral nanocrystals and hierarchical chirality. *J. Am. Chem. Soc.* **2017**, *139*, 6070–6073.
[72] Dicke, R. H. Coherence in spontaneous radiation processes. *Phys. Rev.* **1954**, *93*, 99–110.
[73] Vrehen, Q. H. F.; Schuurmans, M. F. H.; Polder, D. Superfluorescence: Macroscopic quantum fluctuations in the time domain. *Nature* **1980**, *285*, 70–71.
[74] Rainò, G.; Becker, M. A.; Bodnarchuk, M. I.; Mahrt, R. F.; Kovalenko, M. V.; Stöferle, T. Superfluorescence from lead halide perovskite quantum dot superlattices. *Nature* **2018**, *563*, 671–675.
[75] Loudon, R. Photon bunching and antibunching. *Phys. Bull.* **1976**, *27*, 21–23.
[76] Lv, B. H.; Zhang, H. C.; Wang, L. P.; Zhang, C. F.; Wang, X. Y.; Zhang, J. Y.; Xiao, M. Photon antibunching in a cluster of giant CdSe/CdS nanocrystals. *Nat. Commun.* **2018**, *9*, 1536.